

Mechanical properties and oxidation resistance of MoSi₂ and MoSi₂-SiC by a spark plasma sintering process

Min-hyeok Yang^{a,b}, Bum-soon Park^{a,b}, Yu-gyun Park^{a,b}, Ik-hyun Oh^a and Hyun-kuk Park^{a,*}

^aPurpose Built mobility group, Korea Institute of Industrial technology, Gwangju 61012, Republic of Korea

^bDivision of Advanced Materials Engineering, Chonnam National University, Gwangju 61186, Republic of Korea

The MoSi₂ and MoSi₂-SiC were consolidated by a spark plasma sintering process to enhance their mechanical and oxidation resistance properties. The powders were quantified based on the phase diagram and milled using a high energy ball milling. The milled powders were sintered by a spark plasma sintering process at 1300 °C under 60 MPa and heating rate of 100 °C/min. The crystallite size of MoSi₂ and MoSi₂-SiC, using diffraction patterns, were calculated 204.1 and 182.7 nm, respectively. The vickers hardness of MoSi₂ and MoSi₂-SiC are 841.0 and 1067.6 kg/mm², respectively, and the fracture toughness values are 6.53 and 7.08 MPa·m^{1/2}. The SiC present in the MoSi₂ matrix enhanced the mechanical properties of the matrix and increased the fracture toughness by reducing the length of crack propagation. The MoSi₂ and MoSi₂-SiC samples were oxidized by heating to 1000 °C in an oxygen atmosphere. Additionally, the oxidation resistance properties were closely investigated based on the presence of SiC, through the examination of any newly formed phases and the degree of oxygen penetration into the sample surface.

Keywords: MoSi₂, SiC, Spark plasma sintering, Mechanical properties, Oxidation behavior.

Introduction

Structural intermetallic compounds are being researched as new approaches for industrial and military applications alongside the rapid development of aerospace technology. MoSi₂ is recognized as an intermetallic compound used in structural components such as high-temperature heat exchangers, filters, turbine blades, combustors, and nozzles in power generation facilities, gas turbines, and jet engines. Additionally, MoSi₂ has high hardness and a high elastic modulus, providing excellent wear resistance. However, the most intermetallic compounds, such as MoSi₂, exhibit extreme brittleness and low impact strength at elevated temperatures, leading to a decrease in strength and creep resistance. Therefore, it is essential to improve room-temperature fracture toughness, elevated-temperature strength, and creep resistance. Additionally, incorporating additional phase reinforcements can enhance both strength and toughness [1-3]. Recently, a large number of ceramic reinforcements, such as SiC [4], Al₂O₃ [5], TiC [6], and AlN [7] are widely used to strengthen metal matrices for enhancing mechanical properties. In particular, SiC is widely used due to its high wear resistance, excellent mechanical properties at high temperature range, and

low cost. It is reported that SiC does not react with the matrix at elevated temperatures and does not form secondary phases [4].

A variety of processes have been used to fabricate MoSi₂ powder and matrix, including solid-state reaction [8], spray forming [9], mechanical alloying [10], self-propagating high-temperature synthesis (SHS) [11], and spark plasma sintering [12-15]. In particular, the spark plasma sintering process is increasingly used for the production of metals, ceramics, and composites. The spark plasma sintering process differs from conventional sintering methods, where materials receive heat from an external heat source. By directly transmitting current through the powder, temperature differences between the inside and outside were minimized, resulting in uniform physical properties. Additionally, the spark plasma generated on the particle surfaces has a cleaning effect that removes oxide layers and impurities, allowing for sintering at low temperatures and preventing unnecessary reactions between different phases [16].

In this study, Mo and Si powders, as well as Mo₂C, and Si powders, were milled using a high energy ball milling (HEBM) to refine the powders. By inducing a chemical reaction through the spark plasma sintering process, an attempt was made to fabricate the MoSi₂ matrix. The sintering behavior, microstructure, mechanical properties, and oxidation resistance of the sintered body were measured, and the effects of SiC on the mechanical properties and oxidation resistance of the MoSi₂ matrix were compared and analyzed.

*Corresponding author:
Tel: +82-62-600-6270
Fax: +82-62-600-6149
E-mail: hk-park@kitech.re.kr

Experimental Procedure

Mo (45 μm , purity >99.5%, Alfa Aesar), Mo_2C (<44 μm , purity >99.5%, Alfa Aesar), and Si (75 μm , purity 99.9%, Kojundo Chemical Laboratory Co., LTD.) powders were used as the starting materials. Mo + Si and Mo_2C + Si powders were quantified based on the phase diagram. These powders were milled by a high energy ball milling (HEBM, Pulverisette 7, Fritsch) using stainless steel balls with a ball-to-powder weight ratio (BPR) of 10:1. The milling process was performed for 10 hrs at 250 rpm, involving milling for 50 min and a relaxation time of 10 min. The particle sizes of the milled powders (Mo + Si, Mo_2C + Si) were measured as 2.762 and 2.809 μm , respectively using a particle analyzer (Mastersizer 2000E, Malvern Instruments).

The mixed powders were filled in a graphite mold (outer diameter : 30 mm \varnothing , inner diameter : 10 mm \varnothing , height: 40 mmT), respectively, and then the upper and lower parts were blocked with a graphite punch. A vacuum state of about 5 Pa was formed in the chamber. The temperature inside the isothermal temperature was measured using a pyrometer thermal imaging camera, and a initial pressure of 10 MPa was applied. The powder-filled graphite mold was sintered by a spark plasma sintering process (SPS 9.40 MK-III, Sumitomo Heavy Industries) at 1300 $^\circ\text{C}$ under 60 MPa and heating rate of 100 $^\circ\text{C}/\text{min}$ and maintained 2 min. After sintering was completed, the applied pressure was removed after cooling to 200 $^\circ\text{C}$ in the chamber.

The fabricated sintered bodies were measured for relative density using the Archimedes method, and the presence of secondary phases in the sintered body was examined using X-ray diffraction (XRD, X'pert PRO, Malvern Panalytical) equipment. The surface of the sintered body was finely polished using SiC paper, followed by etching with an etching solution (hydrofluoric acid 15 mL, distilled water 85 mL) for 1 min. Finally, the microstructure and elemental analysis were conducted using field emission-scanning electron microscope (FE-SEM)

The hardness was measured using a vickers hardness tester (HV-100, Mitutoyo) by applying a load of 10 kg $_f$ for approximately 7-8 sec. To reduce the standard deviation of the Vickers hardness was measured at 10 \times 10 points with uniform spacing on the surface (0.7 mm horizontally and 0.7 mm vertically). The hardness and fracture toughness were calculated using the diagonal lengths of the generated indentations with Eq. (1) and (2), respectively.

$$H_v = 2 F \sin(136/2) / d^2 \quad (1)$$

$$K = 0.016(E/H_v)^{1/2} (F/C)^{3/2} \quad (2)$$

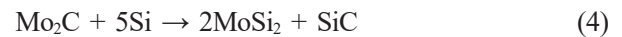
Here, H_v is the vickers hardness, F is the load applied to the sample, d is the diagonal length of the generated

indentation, K is the fracture toughness, E is the elastic modulus, and C is the average length of the crack.

The surface of the fabricated sintered body was heated up to 1000 $^\circ\text{C}$ in an oxygen atmosphere. The phase transformation, microstructure, and the oxide layer of the MoSi_2 matrix were investigated and analyzed according to presence or absence of SiC.

Result and Discussion

Fig. 1 shows the changes in the shrinkage displacement of the sintered body as a function of sintering temperature and time. The fabricated sintered bodies were quantified and sintered according to reaction Eq. (3) and (4) using raw powders.



As the temperature increased, the milled powder reduced its free energy, forming necks between particles, which leads to an increase in shrinkage. MoSi_2 is generally known to form between 1200 and 1400 $^\circ\text{C}$ [17]. In Fig. 1, both sintered bodies showed shrinkage occurring at temperatures above 800 $^\circ\text{C}$. In the temperature range above 1200 $^\circ\text{C}$, expansion rather than shrinkage occurred (see blue line). This indicates that the temperature exceeded the formation temperature of MoSi_2 during the densification process of Mo and Si particles, resulting in a change in volume. In the case of MoSi_2 -SiC (see black line), Mo_2C decomposed into Mo and C above approximately 1000 $^\circ\text{C}$, and MoSi_2 and SiC are formed at temperature above 1200 $^\circ\text{C}$. The relative densities of the two sintered bodies (MoSi_2 and MoSi_2 -SiC) consolidated at 1300 $^\circ\text{C}$ were measured to be 98.08 and 98.22%, respectively. According to study of H. Shimizu [18], the grain growth of the MoSi_2 matrix started above 1400 $^\circ\text{C}$, with a rapid increase in grain size up to 1500 $^\circ\text{C}$. Therefore, sintering above 1400 $^\circ\text{C}$ indicated that it is challenging to produce a high-density

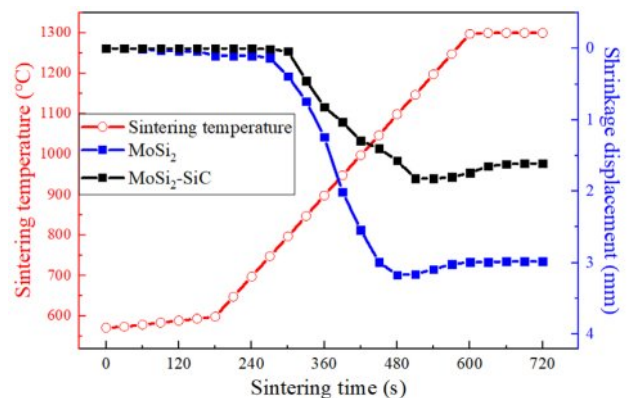


Fig. 1. Sintering behavior as a function of sintering temperature of MoSi_2 and MoSi_2 -SiC.

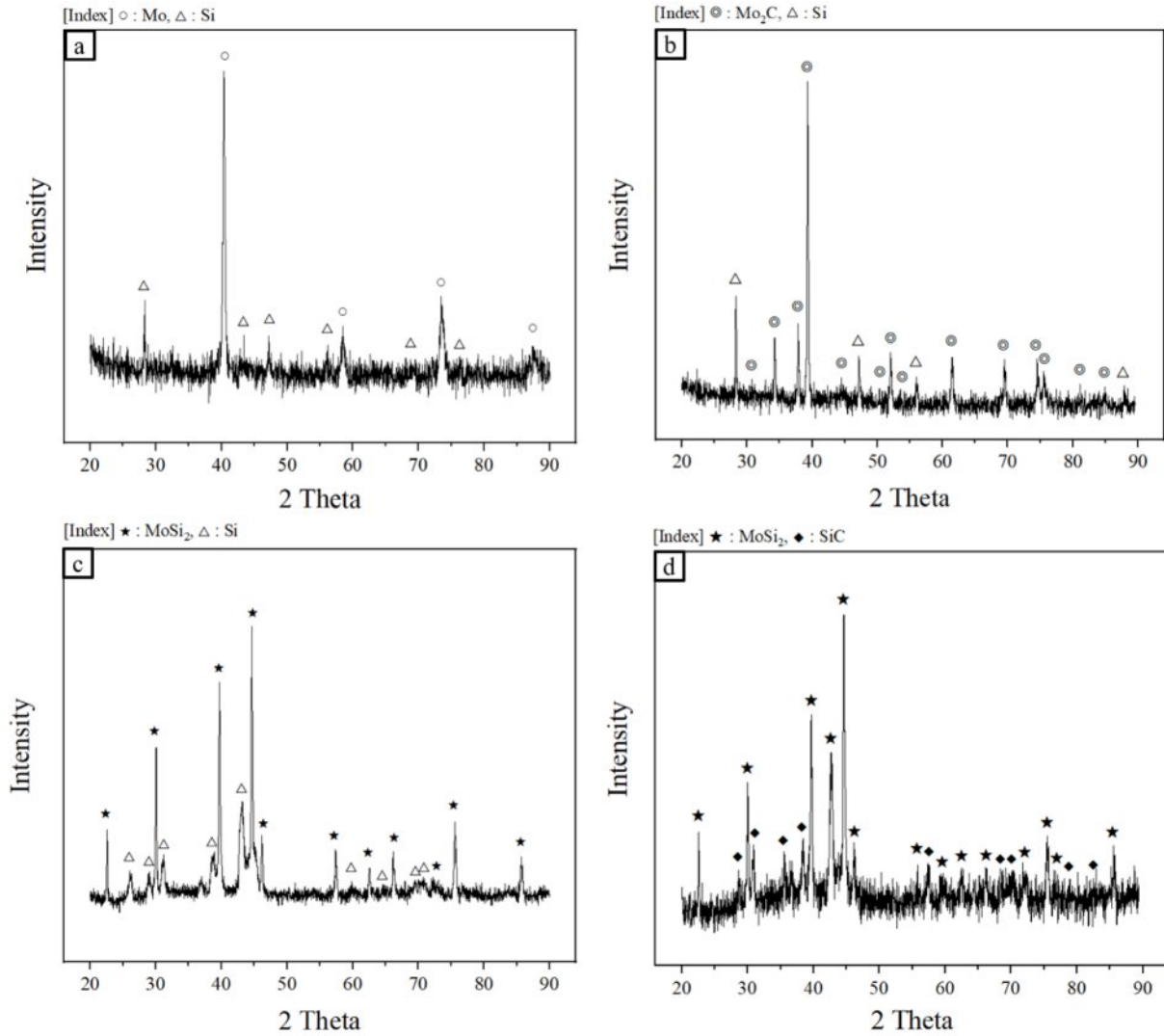


Fig. 2. XRD patterns of mixed powders; (a) $\text{Mo}+\text{Si}$, (b) $\text{Mo}_2\text{C}+\text{Si}$ and sintered bodies; (c) MoSi_2 , (d) $\text{MoSi}_2\text{-SiC}$.

sintered body.

Fig. 2 shows the phase analysis results of the sintered bodies (MoSi_2 and $\text{MoSi}_2\text{-SiC}$) fabricated by a spark plasma sintering process before and after sintering. Before sintering, peaks of Mo , Si , and Mo_2C were predominant; however, after sintering, peaks of MoSi_2 and SiC were observed to be dominant. This indicated that the sintering conditions set in the experiment are suitable for forming MoSi_2 and SiC according to Eq. (3) and (4). In the case of samples produced by hot pressing [17], the formation of Mo_5Si_3 and SiO_2 is unavoidable. In this study, oxide peaks or secondary phases were not detected. This is a result of the spark plasma sintering process, specifically the short sintering time of 13 min at relatively low temperatures under a high vacuum of 5 Pa.

The X-ray diffraction peaks ideally should have a sharp shape with no width, however, in reality, the broadening of XRD peaks occurs due to various factors. In particular, the width of the diffraction peaks is primarily influenced by the crystallite size.

$$\beta_1 = K\lambda/D\cos\theta \quad (5)$$

here, β_1 is the mechanically corrected value of the full width at half maximum (FWHM) of the diffracted X-ray peak, K is the Scherrer constant (≈ 0.9), λ is the wavelength of the X-ray ($\text{CuK}\alpha$, $\lambda=1.54 \text{ \AA}$), and D is the crystallite size. The broadening of the diffraction peaks due to crystallite size can be expressed by the Scherrer equation. However, the Scherrer equation has limitations as it only accounts for the broadening of diffraction peaks due to crystallite size. Therefore, a method that considers both crystallite size and lattice strain is necessary, leading to the development of the Williamson-Hall plot method. The increase in the FWHM of the diffraction peaks due to lattice strain can be expressed as shown in Eq. (6).

$$\beta_2 = 4\epsilon\tan\theta \quad (6)$$

here, ϵ is the lattice strain, and β_2 refers to the corrected value of the full width at half maximum (FWHM) of

the X-ray peak due to internal lattice distortion. When considering both the factors related to crystallite size and lattice strain, the FWHM of the diffraction peaks can be expressed as shown in Eq. (7) [19].

$$\beta_t = \beta_1 + \beta_2 = K\lambda/(D\cos\theta) + 4\epsilon\tan\theta \quad (7)$$

using the XRD data (2 Theta, FWHM) and Eq. (7), the crystallite sizes of MoSi₂ and MoSi₂-SiC sintered bodies were about 204.1 and 182.7 nm, respectively. The presence of SiC had effect on the crystallite growth of the MoSi₂ matrix.

Fig. 3(a), (b) show the SEM images of the MoSi₂ matrix and the MoSi₂-SiC composite, respectively. In Fig. 3(a), both the gray and light gray areas represent MoSi₂. In a small region, the darkest point was found, which corresponded to Si detected in the diffraction peaks. In Fig. 3(b), SiC structure like island shape was formed within the dark MoSi₂ matrix. Fig. 3(c), (d) illustrated the indentations made during hardness measurements of the two samples, while Fig. 3(e), (f) showed the crack propagation in each sample. In MoSi₂, both intergranular and intragranular fractures occurred simultaneously as the crack propagated, with the crack

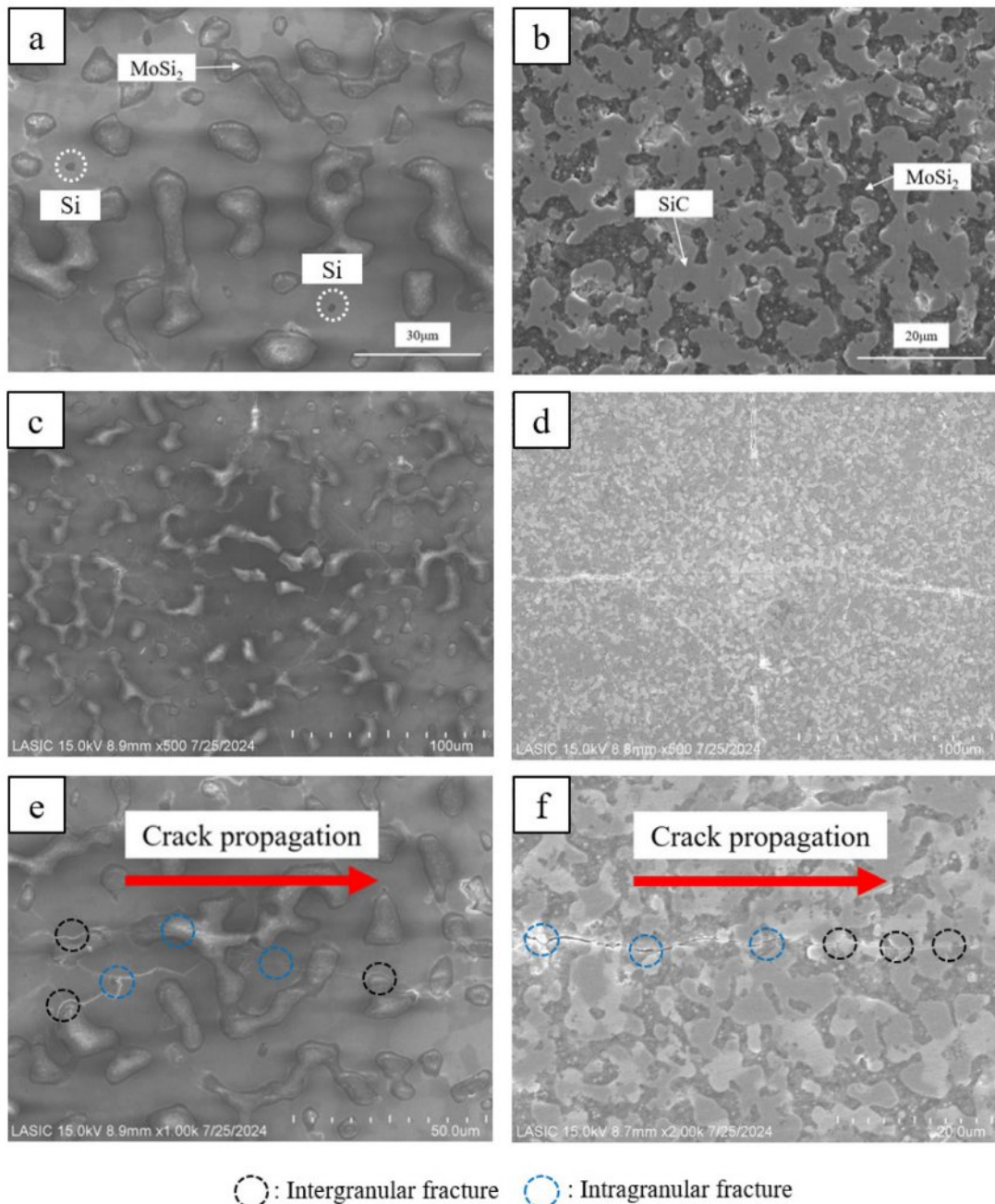


Fig. 3. FE-SEM images of sintered bodies: (a) MoSi₂ and (b) MoSi₂-SiC and cracks propagating from hardness indentations in the sintered bodies: (c), (e) MoSi₂ and (d), (f) MoSi₂-SiC.

Table 1. Vickers hardness and fracture toughness of sintered body.

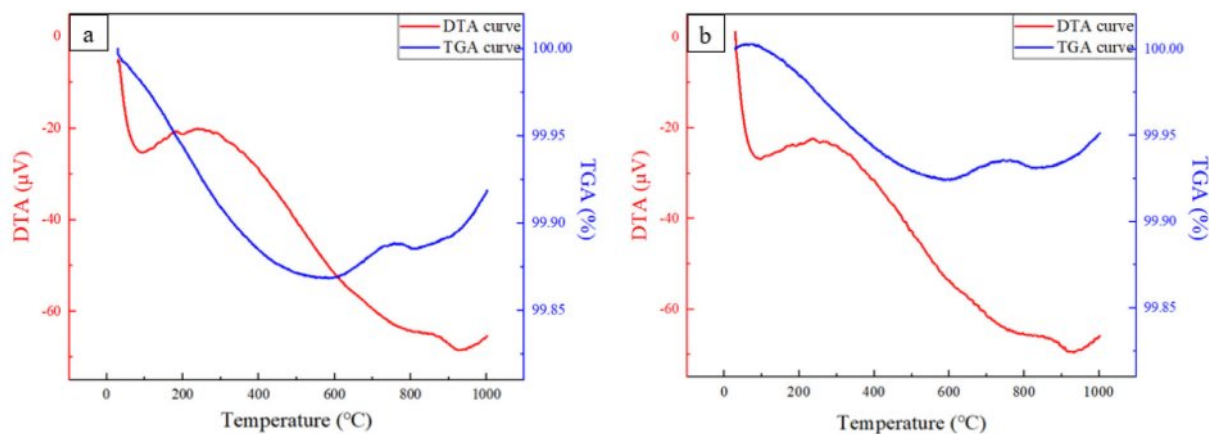
Sintered body	Applied load (kgf)	Average crack length (μm)	Vickers hardness (kg/mm ²)	Fracture toughness (MPa·m ^{1/2})	Elastic modulus (GPa)
MoSi ₂	10	142.96	841.0	6.53	418
MoSi ₂ -SiC	10	125.23	1067.6	7.08	418.8

being extinguished through intragranular fracture at the crack tip. In the case of MoSi₂-SiC, at the initial stage where the crack strength was highest, intragranular fracture occurred in both the MoSi₂ matrix and SiC. As the crack propagated, it advanced towards the boundary between SiC and MoSi₂. In the weaker end of the crack, the crack propagated and was extinguished at the boundary between SiC and MoSi₂.

Table 1 shows the average hardness calculated from 100 indentations generated by a Vickers hardness tester and the fracture toughness calculated using Eq. (1) and (2), respectively. The calculated data indicated that the presence of SiC affects the hardness and fracture toughness of the MoSi₂ matrix. In composite materials, the enhancement of toughness is primarily due to factors such as the boundaries between different phases, the utilization of specific phases for toughness improvement, particle size and distribution, and layered structures. According to the study by D. Sciti [20], the use of Si₃N₄, which has a higher fracture toughness than MoSi₂, has enhanced the fracture toughness of MoSi₂. In this study, the SiC present in the MoSi₂ matrix enhanced the mechanical properties of the matrix and increased the fracture toughness by reducing the length of crack propagation. A higher fracture toughness value means that the material has a greater ability to withstand significant deformation before failure. In other words, it indicates the ability of the material to absorb amount of energy and undergo deformation before cracks occur when external forces or loads are applied, showing that SiC enhanced the ability of the MoSi₂ matrix to withstand deformation.

Fig. 4 shows the changes in endothermic and exothermic reactions and mass during the oxidation of the two sintered bodies in an oxygen atmosphere up to 1000 °C. The decrease in microvolts in differential thermal analysis (DTA) generally has four reasons: the microvolts decreased due to phase changes or chemical reactions within the sample, changes in thermal conductivity can alter the way heat is transferred, and when the temperature of the sample remains stable within a certain range, the lack of thermal changes can lead to a decrease in microvolts [21]. Both MoSi₂ and MoSi₂-SiC exhibited similar patterns of increase or decrease in the graph, with only absolute differences in values, indicating similar behavior. In the low-temperature range (below 100 °C), the relatively stable temperature of both samples resulted in a decrease in thermal changes, leading to a reduction in microvolts. The increase in microvolts between 100 and 300 °C indicated exothermic reactions due to phase changes or chemical reactions within the samples. Above 300 °C, the microvolts continuously decreased, indicating decomposition reactions of MoSi₂ or the formation of SiO₂. The increase in microvolts around 900 °C suggested that the phase change has been completed. Both samples exhibited similar mass change behaviors. Since MoSi₂ is generally heavier than Mo oxides, differences in the extent of decrease were observed.

Fig. 5 shows the phase analysis results of the oxidized samples. In the phase analysis results before oxidation (see Fig. 2), the intensity of the background peak was parallel to the x-axis. However, in the case of the background peak of the oxidized sintered body,

**Fig. 4.** Heat flow and mass change of the sintered bodies: (a) MoSi₂ and (b) MoSi₂-SiC heated up to 1000 °C in an oxygen atmosphere.

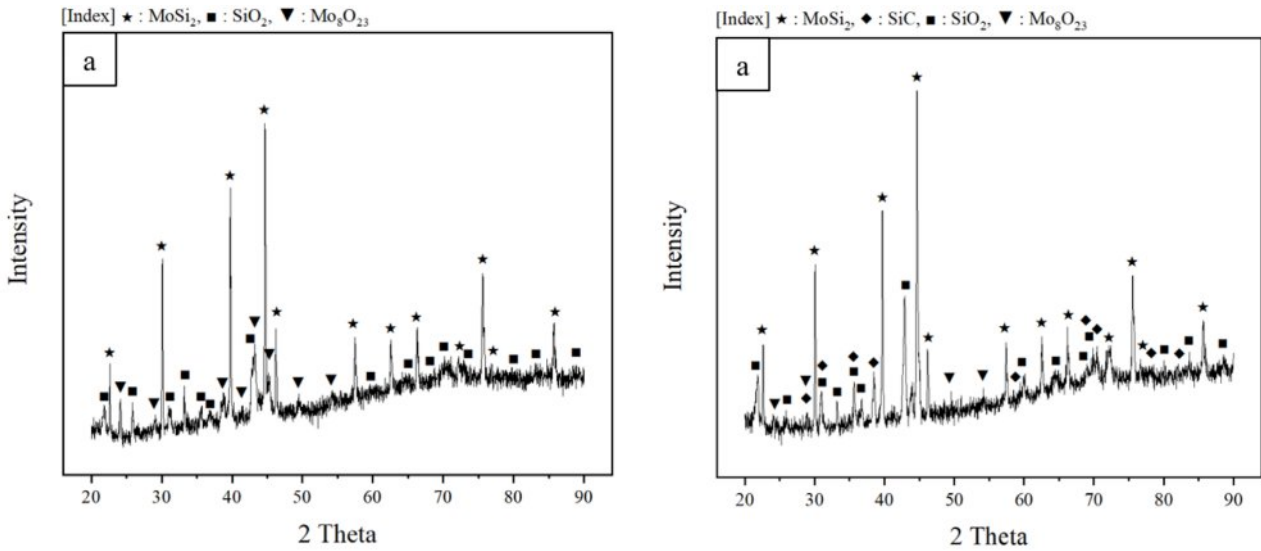


Fig. 5. XRD patterns of the oxidized sintered bodies: (a) MoSi_2 and (b) $\text{MoSi}_2\text{-SiC}$.

Table 2. Quantitative analysis results using diffraction patterns.

Phase (vol.%)	MoSi_2	SiO_2	Mo_8O_{23}	SiC	total
MoSi_2	81.3	15.5	3.2	-	100
$\text{MoSi}_2\text{-SiC}$	52.5	37.0	0.6	9.9	100

the intensity showed a slight increase as the 2 Theta value increased. This is a result of the formation of extra peaks due to the presence of SiO_2 or Mo oxides. The quantitative calculation results for each phase corresponding to the peaks were summarized in Table 2 using the diffraction pattern. In the case of $\text{MoSi}_2\text{-SiC}$, the amount of SiO_2 increased due to SiC during the oxidation process, leading to a relative decrease in the amount of Mo oxides generated. Since the density of Mo oxide is greater than that of SiO_2 , the change in mass for the same volume is determined by the Mo oxides. In the previous TGA curve (see Fig. 4), (a) and (b) showed numerical differences. As a result, it indicated that in the case of MoSi_2 , which generated a larger amount of Mo

oxides during the oxidation process, the mass decreased significantly compared to $\text{MoSi}_2\text{-SiC}$.

Fig. 6 presented the analysis results of the oxide layer for the two oxidized samples. Neither sample formed a noticeable oxide layer. In the study by M. Samadzadeh, oxidation processes were conducted over a range of temperatures (1000-1600 °C). According to the results [22], significant oxide layers were found in MoSi_2 based materials at temperature above 1300 °C. In temperature range below 1300 °C, a distinct oxide layer was not noticeably formed from the surface, resulting in the formation and distribution of Mo oxides and Si oxides on the surface. To observe a clear oxide layer, oxidation processes at higher temperatures are necessary. Based on the detected elemental peaks, the bright areas in (a) correspond to Si oxide or Mo oxide, while most of the darker areas represented the MoSi_2 matrix. Fig. 7 presented the quantitative data of element O from the line profile as a function of distance. By integrating the graph with respect to distance, the integrated area is calculated. The integration result for the distance

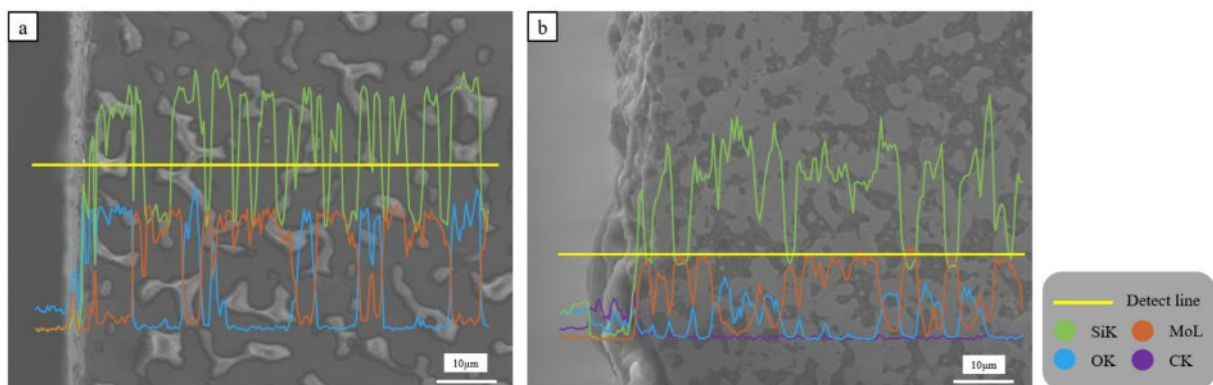


Fig. 6. Microstructure and elemental line profile of the oxide layer in the oxidized sintered bodies: (a) MoSi_2 and (b) $\text{MoSi}_2\text{-SiC}$.

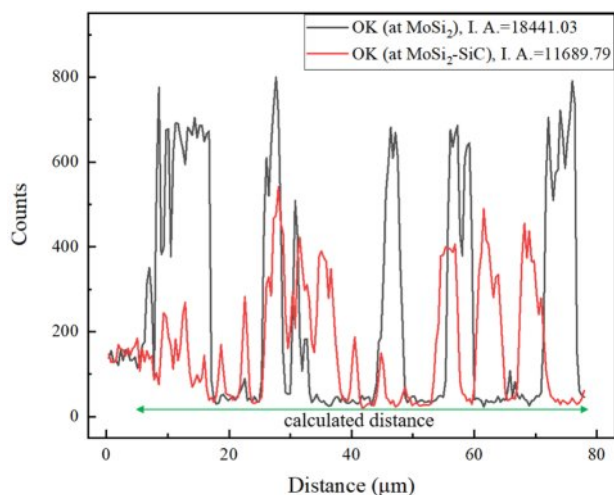


Fig. 7. Quantitative data of oxygen (O) elements line profile from oxidation layer to matrix.

excluding the initial 4 μm of the approximately 80 μm measured line profile (the area not part of the sample) calculated values of 18441.03 for MoSi₂ and 11689.79 for MoSi₂-SiC. These values indicated the oxidation resistance [23]. The presence of SiC distributed in the MoSi₂ matrix relatively reduced the amount of oxidized MoSi₂ (the amount of generated Mo oxides), thereby enhancing the oxidation resistance of the MoSi₂ matrix.

Conclusion

Using Mo, Mo₂C, and Si powders as raw materials, a mixture was prepared through high energy ball milling, and a sintered in a single process and short time by a spark plasma sintering process. The conclusions were as follows:

1. In the case of MoSi₂-SiC, at the initial stage where the crack strength was highest, intragranular fracture occurred in both the MoSi₂ matrix and SiC. As the crack propagated, it advanced towards the boundary between SiC and MoSi₂. Finally, the crack propagated and was extinguished at the boundary between SiC and MoSi₂.
2. The amount of SiO₂ in the case of MoSi₂-SiC increased due to SiC during the oxidation process, leading to a relative decrease in the amount of Mo oxides generated. Since the density of Mo oxide is greater than that of SiO₂, the change in mass for the same volume is determined by the Mo oxides.
3. In temperature range below 1300 °C, a distinct oxide layer was not noticeably formed from the surface, resulting in the formation and distribution of Mo oxides and Si oxides on the surface. The distribution of SiC in the MoSi₂ matrix relatively decreases the amount of MoSi₂, that oxidized, thereby enhancing the oxidation resistance properties.
4. The integration area was calculated values of

18441.03 for MoSi₂ and 11689.79 for MoSi₂-SiC. The presence of SiC distributed in the MoSi₂ matrix relatively reduced the amount of oxidized MoSi₂ (the amount of generated Mo oxides), thereby enhancing the oxidation resistance of the MoSi₂ matrix.

Acknowledgement

This study has been conducted with the support of the Korea Institute of Industrial Technology as “Development of smart electric driving platform by eco-friendly power source in agricultural work environment (KITECH JA-25-0008).

References

1. Y.H. Park, S.P. Lee, S.E. Lee, J.O. Jin, S.W. Kim, J.K. Lee, and H.K. Yoon, *J. Ocean Eng. Technol.* (2003) 289-293.
2. H.K. Park, J.K. Yoon, K.T. Hong, and I.J. Shon, *J. Alloys Compd.* 426 (2006) 322-326.
3. H.K. Park, H.C. Kim, J.K. Yoon, K.T. Hong, I.Y. Ko, and I.J. Shon, *Scr. Mater.* 56 (2007) 665-668.
4. A.P. Kumar, S. Aadithya, K. Dhilepan, and N. Nikhil, *ARPN J. Eng. Appl. Sci.* 11 (2016) 1204-1210.
5. A. Saravanakumar, P. Sasikumar, and S. Sivasankaran, *Procedia Eng.* 97 (2014) 951-960.
6. S. Saravanan, P. Senthilkumar, M. Ravidchandran, and V. Anandakrishnan *J. Mater. Res.* 32 (2017) 606-614.
7. V. Mohanavel, K. Rajan, and M. Ravichandran, *J. Mater. Res.* 31 (2016) 3824-3831.
8. S.W. Jo, M.D. Ka, and Y.S. Kim, *Acta Mater.* 11 (1996) 4317-4326.
9. E.J. Lavernia, *Int. J. Rapid Solidificat.* 5 (1989) 47-85.
10. L. Xiao, Y. S. Kim, and R. Abbaschian, *Mater. Res. Soc. Symp. Proc.* 194 (1990) 399-402.
11. S.C. Deevi, *J. Mater. Sci.* 12 (1991) 3343-3353.
12. T. Nishimura, M. Mitomo, H. Hirotsuru, and M. Kawahara, *J. Mater. Sci. Lett.* 15 (1995) 1046-1047.
13. J.H. Lee, J.C. Park, B.S. Park, and H.K. Park, *J. Ceram. Process. Res.* 24 (2023) 216-221.
14. J.H. Lee and H.K. Park, *J. Ceram. Process. Res.* 22 (2021) 655-664.
15. H.K. Park, I.H. Oh, J.H. Jang, H.T. Shon, H.S. Kim, and I.J. Shon, *J. Ceram. Process. Res.* 17 (2016) 191-196.
16. G. Xie, O. Ohashi, T. Yoshioka, M. Song, K. Mitsuishi, H. Yasuda, K. Furutyand, and T. Noda, *Mater. Trans.* 42 (2001) 1846-1849.
17. J. Liu, Q. Gong, Y. Shao, D. Zhuang, and J. Liang, *Appl. Surf. Sci.* 308 (2014) 261-268.
18. H. Shimizu, M. Yoshinaka, K. Hirota, and O. Yamaguchi, *Mater. Res. Bull.* 37 (2002) 1557-1563.
19. C.H. Lee, *J. Ceram. Process. Res.* 9 (2008) 321-324.
20. D. Sciti, S. Guicciardi, and A. Bellosi, *J. Ceram. Process. Res.* 3 (2002) 87-95.
21. W. Smykatz-Kloss, [Differential thermal analysis: application and results in mineralogy] (2012).
22. M. Samadzadeh, C. Opera, H.K. Sharif, and T. Troczynski, *Int. J. Refract. Met. H.* 69 (2017) 31-39.
23. B.S. Park, J.H. Lee, J.C. Park, and H.K. Park, *J. Alloys Compd.* 984 (2024) 173900.